

DETC2011-4, ) ) +

## CLOSED-FORM SOLUTIONS TO THE KINEMATICS OF A PARALLEL LOCOMOTION MECHANISM WITH ACTUATED SPOKE WHEELS

Ping Ren<sup>1</sup>

RoMeLa: Robotics & Mechanisms Laboratory  
Mechanical Engineering Department  
Virginia Tech  
Blacksburg, Virginia 24061, U.S.A  
Email: renping@vt.edu

Dennis Hong

RoMeLa: Robotics & Mechanisms Laboratory  
Mechanical Engineering Department  
Virginia Tech  
Blacksburg, Virginia 24061, U.S.A  
Email: dhong@vt.edu

### ABSTRACT

A parallel locomotion mechanism can be defined as “a mechanism with parallel configuration that has discrete contact with respect to the ground which renders a platform the ability to move”. The actuated spoke wheel robot IMPASS (Intelligent Mobility Platform with Active Spoke System) presented in this paper serves as an example of such locomotion mechanisms. The current prototype of IMPASS has two actuated spoke wheels and one passive tail with its lower portion designed as convex surface. The robot is considered as a mechanism with variable topologies (MVTs) because of its metamorphic configuration. Closed-form solutions to the kinematics of the variable topologies are developed and verified with numerical simulations. The analytical expressions to these solutions allow themselves to be used directly in the real-time motion planning and monitoring of the robot.

### 1. INTRODUCTION

One focus of today’s robotics science and technology is to develop novel locomotion mechanisms that possess adequate mobility in various environments. With the implementation of appropriate locomotion schemes, mobile platforms can perform those tasks that are dirty, dull, dangerous or inaccessible to human beings, such as scientific exploration of remote areas, military surveillance, search and rescue missions and so on. The locomotion of traditional manned ground vehicles mainly includes wheels, tracks and hybrid combinations of both. However, the growing demand for lightweight mobile robots calls for innovative concepts on alternative locomotion.

The scientific study on legged locomotion as an alternative to wheels and tracks began over a century ago, and a human-

controlled, four-legged walking machine with adjustable gaits was firstly built at General Electric in mid-1960s, as was introduced in Ref. [1]. Through the viewpoint of modern kinematics, wheeled or tracked vehicles are inherently different from legged walking machines in that the former always maintain continuous contact with the ground while the latter have discrete contact with the ground. Additionally, in any of its stable configurations, the body or platform of the walking machine is always connected to the ground through multiple in-parallel branches. As the legs or branches are lifted above and put down, the body is moved from place to place. Meanwhile, as the machine walks, the location and geometry of the virtual base formed by the contact feet on the ground change as well.

Based on the discussion above, a class of alternative locomotion mechanisms can be proposed which distinguish themselves by their kinematically parallel configurations. A *parallel locomotion mechanism can be defined as “a mechanism with parallel configuration that has discrete contact with respect to the ground which renders a platform the ability to move”* [2]. Another important and necessary characteristic of a parallel locomotion mechanism is its ability to change topologies. Usually, a parallel locomotion mechanism has more than one topology; when a branch is lifted above the ground, the topology of the mechanism changes correspondingly, as well as the geometry of its virtual base on the ground. For such locomotion mechanisms, a fundamental research on their kinematics is quite necessary, as it will lay the foundation for other studies such as design optimization, dynamics modeling, nonlinear control, motion planning and so on.

<sup>1</sup> Address all correspondence to this author.

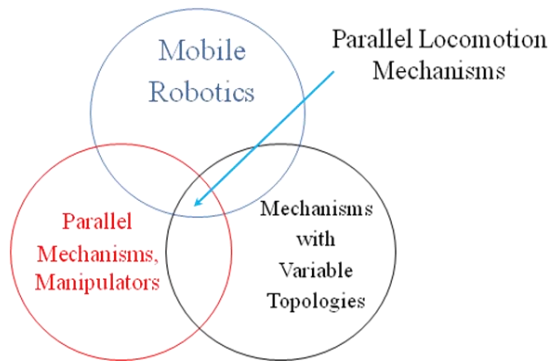


**Figure 1** The relationship of Parallel Locomotion Mechanism (PLM) with Related Disciplines

As shown in Figure 1, Parallel Locomotion Mechanism (PLM) is a new interdisciplinary area which requires background knowledge in mobile robotics, parallel manipulators, and mechanisms with variable topologies. Two mobile robots with such locomotion mechanisms are currently under development at RoMeLa: Robotics and Mechanisms Laboratory in Virginia Tech. Previous research works can be found in Refs. [3-8]. The first robot STrIDER (Self-excited Tripedal Dynamic Experimental Robot) is a three-legged robot that utilizes its built-in passive dynamics for walking. The kinematics in its triple stance phase has been investigated in Refs. [3]. The second robot IMPASS (Intelligent Mobility Platform with Active Spoke System) is an actuated spoke wheeled robot that has various topologies with respect to the ground. The uniqueness of this type of spoke wheels is that each spoke can be actuated to stretch in or out independently.

The IMPASS robot serves in this paper mainly as an example to the kinematics study on parallel locomotion mechanisms. The content of the paper is organized as: the background of the IMPASS robot with two spoke wheels and one tail is introduced in Section 2; followed by the forward and inverse kinematics analysis in Section 3. In Section 4, examples based on simulations are presented to verify the closed-form solutions obtained. Finally, conclusions are summarized and future research is briefly discussed in Section 5.

## 2. BACKGROUND

Leg-wheel hybrid robots have been drawing more attention since they have the advantages of both legs and wheels. Legged locomotion is more adaptable to a wide range of unstructured grounds but the complicated mechanism of the legs is very difficult to implement. On the other hand, wheeled locomotion is fast and efficient but it tends to be limited to relatively smooth terrain. Therefore, in order to create a walking machine that combines the benefits of both locomotion schemes, spoke wheels or similar mechanisms could be good candidates.

Previous mobile platforms that utilize compliant spoke wheels mainly included RHex [9] and Whegs<sup>TM</sup> [10]. RHex was

a compliant-legged hexapod with a simple clock-driven open-loop tripod gait. It was different from other mobile robots in that each of its legs rotated in full circles acting as a single spoke wheel. The Whegs<sup>TM</sup> series of robots was the another derivation of the spoke wheel concept that utilized compliant tri-spoke configuration in each wheel.

**2.1 Intelligent Mobility Platform with Active Spoke System.** As a novel concept for creating a series of hybrid mobile robots with robust mobility, the architecture of a rimless wheel with multiple extensible spokes passing through the center was proposed as early as in Ref. [11]. The IMPASS robot presented in this paper was conceived independently [4, 5], but is also based on the similar concept. Compared with the aforementioned RHex and Whegs<sup>TM</sup> robots, the major difference of the IMPASS lies on the mechanism of its spoke wheels (six spokes per wheel unit, compared to three for Whegs<sup>TM</sup> and only one for RHex), and its ability to stretch each spoke in or out intelligently. The latest IMPASS prototype demonstrated in Figure 2 has two actuated spoke wheels and one passive tail. The spokes are made of carbon fibers and set 60 degrees from each other. The body is covered with a carbon fiber shell. The shell has a tail, with its lower portion designed as a convex surface. As the robot walks on various terrains, climbs up steps and so on, the tail together with the spokes that contact the ground can provide a support region to maintain its stability.

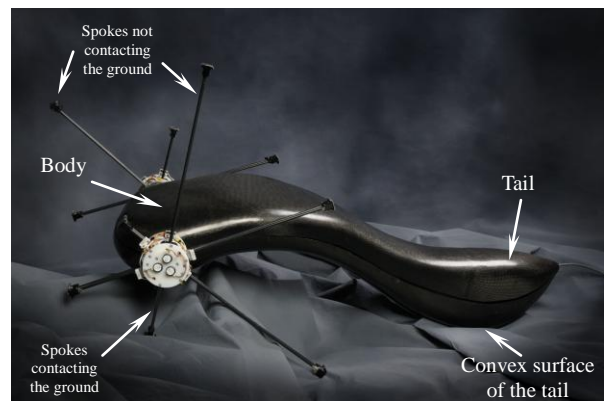


**Figure 2** The prototype of IMPASS

As the IMPASS moves on smooth surfaces, its body is always connected to the ground through multiple actuated spokes. Therefore, by treating the ground as the base and the spokes as the limbs, this mobile robot can be considered as a parallel locomotion mechanism, as well as a mechanism with variable topologies (MVTs). Each of its topological structures is characterized by the contact scheme of the spokes. The variable mobility, i.e. the metamorphic degrees of freedom (d.o.f.) possessed by the robot's body, was identified in Ref. [6] for all cases of its topologies. As a follow-up, Ref. [7] revealed that the ground motions of the IMPASS, such as straight-line walking, steering and other combinations, could be uniformly

interpreted as a series of topological transformations. This paper is intended to investigate the forward and inverse kinematics for such topologies in order to further understand their characteristics.

**2.2 Kinematic Configuration.** For convenience, a simple and straightforward nomenclature is composed to describe the contact case in each topology [6]. This nomenclature generally follows the format of “ $n_1$ - $n_2$ : parallel & equal / parallel & unequal / skew”. The term “ $n_1$ - $n_2$ ” is used to represent the numbers of the contacting spokes in the left and right wheels respectively, with the term “parallel & equal / parallel & unequal” indicating whether or not the geometrically parallel contacting spokes in this case are of equal length. The term “skew” is used only when the left contacting spoke is skew to the right contacting spoke.

As an example, the characteristic geometry of the IMPASS prototype in Figure 2 is extracted, and represented with the kinematic model shown in Figure 3. In this case, two spokes from the left and right wheel respectively and the tail are contacting the smooth ground. This case can be addressed as “1-1: parallel & equal” because the left contacting spoke is parallel and equal to the right one. Note that the contacting and un-contacting spokes are represented with solid and transparent cylinders respectively in this figure.

In the case shown in Figure 3, the two spoke wheels are connected with an axle. So the actuation of this robot is the rotation of the spoke wheels about the axle in the direction indicated by the double arrow in this figure, and the translations of the contacting spokes through the hub of the wheel. The un-contacting spokes can also stretch in or out locally, but their displacements do not affect the configuration of the robot in its current topology, unless they touch the ground thus changing its topology.

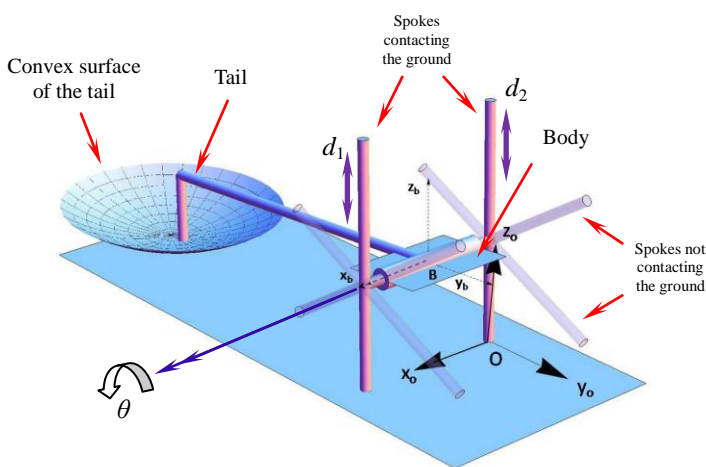


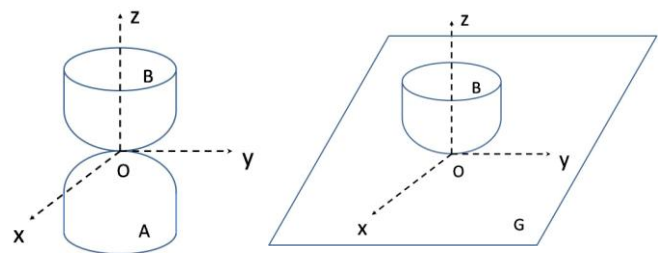
**Figure 3** Kinematic model of IMPASS with two spokes and the tail in contact with the smooth ground (1-1: parallel & equal)

The geometry of the body and tail is simplified, and represented with a rectangle plane connecting to a convex surface through a rigid link. At present, the convex surface of the tail is designed as part of a spherical surface, but other types of convex surfaces such as hyperboloid of two sheets, paraboloid etc., might be considered in the future. The body and tail as a whole is attached to the axle that actuates the two spoke wheels. Through moderate modifications, this model can also be used to demonstrate other contact cases in Ref. [6].

### 3. FORWARD AND INVERSE KINEMATICS ANALYSIS

As the robot walks on various terrains, its tail passively touches the ground. Therefore, at any instant, there exist at least three contact points between the IMPASS and the ground (two or more come from the contacting spokes, and one or more from the tail). For the various contact cases, the objective of the forward and inverse kinematics is to investigate the geometric relationships of the body’s position/orientation and the joint variables. In this paper, the scope of the kinematics analysis is confined to the smooth ground. A few assumptions are made ahead, which include:

1. The IMPASS robot consists of rigid links, such as the spokes and the axle. Especially, the body and tail as a whole is considered as one rigid link;
2. The two spoke wheels rotate in the same phase, so for each spoke in the left wheel, there is always a parallel spoke in the right wheel;
3. When a spoke touches the ground, the generated contact point is kept stationary, i.e. no slip or bounce occurs at the contact tips as the contacting spokes rotate or translate. Each contacting spoke is modeled as a limb consisting of a Spherical-Prismatic (SP) dyad;
4. The tail’s passive touching with the smooth ground generates one contact point only, since the lower portion of the tail is a partial spherical surface. This contact point is treated as the tangential point between the spherical surface and the ground plane. Because the tail and the ground are both rigid and contacting each other at one point, a *surface contact pair* is thus generated [12]. As illustrated in Figure 4, the two contacting surfaces are free to roll and slide with respect to one another as long as the contact point is maintained, so this pair is a higher pair with five d.o.f



(a)  
(b)

**Figure 4** Surface contact pair

Please note that, the following analysis mainly focuses on the “1-1” contact cases. Other contact cases in Ref. [6] have only one d.o.f. or no d.o.f.. Compared with the “1-1” cases, their kinematics is relatively simple.

**3.1 Forward Kinematics.** Forward kinematics analysis aims to calculate the position and orientation of the robot’s body with given joint displacements. Among all cases of its topologies, the “1-1” cases with two spokes and the tail in contact with the ground possess two d.o.f and contribute the most to its locomotion [7]. Considering the topology of the IMPASS robot shown in Figure 3, the joint variables that can be specified are the angular displacement of the two spoke wheels and the linear displacement of the two contacting spokes. Since the rotation of the two wheels is in phase and the translations of the two spokes are dependent on each other, there are two d.o.f in this topology.

Given the presumption that three non-collinear contact points exist (two from the contacting spokes and one from the tangency of the tail’s lower surface with the smooth ground), the forward kinematics of the IMPASS robot in this contact case can be formulated through the following procedures.

First, as shown in Figure 3, two coordinate systems are established with  $\{x_o, y_o, z_o\}$  fixed on the ground and  $\{x_b, y_b, z_b\}$  attached to the robot’s body. The origin O of  $\{x_o, y_o, z_o\}$  is chosen at the contact point between the left spoke and the ground, with  $x_o$  axis pointing to the right contact point and  $z_o$  axis normal to the ground. The origin B of  $\{x_b, y_b, z_b\}$  is set at the midpoint of the axle, with  $x_b$  axis pointing to the right wheel center, also the direction of the spoke wheels’ rotation, and  $y_b$  axis lying in the rectangle plane and pointing to the front of the body.

Secondly, assume the body coordinate system  $\{x_b, y_b, z_b\}$  is positioned at the global origin with zero orientation, then with given joint displacements, the position vectors of the contact points of the two spokes ( $\mathbf{P}_1$  and  $\mathbf{P}_2$ ) with respect to the body frame can be determined using homogenous coordinates and transformation matrices as follows:

$$\begin{bmatrix} \mathbf{P}_1 \\ 1 \end{bmatrix} = R_x(\theta) \begin{bmatrix} \mathbf{p}_1 \\ 1 \end{bmatrix} \quad (1)$$

and

$$\begin{bmatrix} \mathbf{P}_2 \\ 1 \end{bmatrix} = R_x(\theta) \begin{bmatrix} \mathbf{p}_2 \\ 1 \end{bmatrix} \quad (2)$$

where

$$R_x(\theta) = \begin{bmatrix} 1 & 0 & 0 & 0 \\ 0 & \cos\theta & \sin\theta & 0 \\ 0 & -\sin\theta & \cos\theta & 0 \\ 0 & 0 & 0 & 1 \end{bmatrix} \quad (3)$$

$$\mathbf{p}_1 = [l_a/2 \quad 0 \quad -d_1]^T$$

$$\mathbf{p}_2 = [-l_a/2 \quad 0 \quad -d_2]^T$$

In Eqs.(1-3),  $l_a$  is the length of the axle;  $\theta$  is the angular displacement of the two spoke wheels;  $d_1$  and  $d_2$  are the linear displacements of the left and right contacting spokes respectively, measured from the centers of the wheels to the contact points.  $d_1$  and  $d_2$  must comply with the following constraint:

$$d_1 - d_2 = \Delta d \quad (4)$$

where  $\Delta d$  is a non-zero constant for “1-1: parallel & unequal” case and zero for “1-1: parallel & equal” case. It is usually determined by the initial condition of the contact cases. The constraint of Eq.(4) is to ensure that the distance between the two spoke contact points is constant in its current topology, such that slip or bounce does not occur at the spoke tips.

As for the “1-1: skew” case in which the two contacting spokes are skew to each other with the twisting angle of 60 degrees, Eq.(2) needs to be modified as:

$$\begin{bmatrix} \mathbf{P}_2 \\ 1 \end{bmatrix} = R_x(\theta + \pi/3) \begin{bmatrix} \mathbf{p}_2 \\ 1 \end{bmatrix} \quad (2)^*$$

and  $d_1, d_2$  should follow the quadratic constraint as follows:

$$d_1^2 - d_1 d_2 + d_2^2 = e^2 - l_a^2 \quad (4)^*$$

where  $e$  is the distance between the two contact points,  $l_a$  is again the length of the axle and both of them are constants. The detailed derivation of Eq.(4)\* and discussions on the skew contact case can be found in Ref. [8].

Thirdly, with  $\mathbf{P}_1$  and  $\mathbf{P}_2$  calculated from Eqs.(1-3) or Eq.(1),(2)\* and (3), the position vector of  $\mathbf{P}_3$  with respect to the body coordinates  $\{x_b, y_b, z_b\}$  can now be determined by finding the tangential point between the spherical surface of the tail and the ground plane that contains points  $\mathbf{P}_1$  and  $\mathbf{P}_2$ . Assuming the function of the surface in the body coordinate system is  $F(x, y, z) = 0$ , then the equations to obtain  $\mathbf{P}_3$  can be formulated as follows:

$$F(P_{3x}, P_{3y}, P_{3z}) = 0 \quad (5.1)$$

$$F'_x(P_{3x}, P_{3y}, P_{3z})(P_{1x} - P_{3x}) + F'_y(P_{3x}, P_{3y}, P_{3z})(P_{1y} - P_{3y}) \quad (5.2)$$

$$+ F'_z(P_{3x}, P_{3y}, P_{3z})(P_{1z} - P_{3z}) = 0$$

$$F'_x(P_{3x}, P_{3y}, P_{3z})(P_{2x} - P_{3x}) + F'_y(P_{3x}, P_{3y}, P_{3z})(P_{2y} - P_{3y}) \quad (5.3)$$

$$+ F'_z(P_{3x}, P_{3y}, P_{3z})(P_{2z} - P_{3z}) = 0$$

where  $P_{ix}, P_{iy}, P_{iz}$  are the three components of  $\mathbf{P}_i$ , with  $i = 1, 2, 3$  and  $\mathbf{P}_i = [P_{ix}, P_{iy}, P_{iz}]^T$ .  $F'_x, F'_y$  and  $F'_z$  in Eq.(5.2) and Eq.(5.3) are the partial derivatives of  $F(x, y, z)$  with respect to  $x, y$ , and  $z$  respectively. Eqs.(5.1-5.3) all have definite geometric

meanings. Eq.(5.1) ensures that  $P_3$  is on the surface, while Eq.(5.2) and Eq.(5.3) guarantee that the tangential plane i.e. ground plane, at  $P_3$  also passes  $P_1$  and  $P_2$ . With  $\mathbf{P}_1$  and  $\mathbf{P}_2$  known, Eqs.(5.1-5.3) now become an equation system with three unknowns  $P_{3x}, P_{3y}, P_{3z}$ , thus  $\mathbf{P}_3$  is solvable.

Finally, with  $\mathbf{P}_1, \mathbf{P}_2$  and  $\mathbf{P}_3$  obtained, the configuration of the ground plane relative to the body coordinate system is determined definitely. The three orthogonal unit vectors describing the orientation of the ground can be found as:

$$\begin{aligned} \mathbf{x}'_o &= (\mathbf{P}_1 - \mathbf{P}_2) / \|\mathbf{P}_1 - \mathbf{P}_2\| \\ \mathbf{z}'_o &= \mathbf{x}'_o \times (\mathbf{P}_2 - \mathbf{P}_3) / \|\mathbf{x}'_o \times (\mathbf{P}_2 - \mathbf{P}_3)\| \\ \mathbf{y}'_o &= \mathbf{z}'_o \times \mathbf{x}'_o \end{aligned} \quad (6)$$

The ground coordinate system  $\{x_o, y_o, z_o\}$  has its origin at point  $P_2$ , so the homogeneous transformation matrix from the ground frame to the body frame is established as:

$$\mathbf{H}_B^O = \begin{bmatrix} \mathbf{x}'_o & \mathbf{y}'_o & \mathbf{z}'_o & \mathbf{P}_2 \\ 0 & 0 & 0 & 1 \end{bmatrix} \quad (7)$$

By taking the inverse of the matrix  $\mathbf{H}_B^O$ , the configuration of the body attached frame  $\{x_b, y_b, z_b\}$  with respect to the ground fixed frame  $\{x_o, y_o, z_o\}$  is obtained as:

$$\begin{aligned} \mathbf{H}_O^B &= (\mathbf{H}_B^O)^{-1} = \begin{bmatrix} [\mathbf{x}'_o & \mathbf{y}'_o & \mathbf{z}'_o]^T & -[\mathbf{x}'_o & \mathbf{y}'_o & \mathbf{z}'_o]^T \mathbf{P}_2 \\ \mathbf{0} & & & 1 \end{bmatrix} \\ &= \begin{bmatrix} \mathbf{x}_b & \mathbf{y}_b & \mathbf{z}_b & \mathbf{B} \\ 0 & 0 & 0 & 1 \end{bmatrix} \end{aligned} \quad (8)$$

Thus, the forward kinematics of IMPASS with two spokes and the tail in contact with the ground is formulated completely. With given joint displacements, i.e.  $\theta, d_1$  and  $d_2$ , the position and orientation of IMPASS' body with respect to the ground are obtained and represented with the homogeneous transformation matrix  $\mathbf{H}_O^B$  in closed-forms. Theoretically, it is possible that the forward kinematics has multiple solutions. Inspecting the kinematic model of the IMPASS robot in Figure 3, the multiple solutions are due to the existence of multiple tangential points between the spherical surface and the ground plane, i.e. the whole spherical surface at the tail can have two tangential points with the plane that passes line  $P_1P_2$ , resulting in two forward kinematics solutions. However, the additional solution can be easily eliminated because only the lower portion of the spherical surface is real and the tangential point at the upper portion does not exist in the physical model and thus unique solution will be derived.

The procedures discussed above not only solve the forward kinematics in the topology of the robot that has two spokes and the tail contacting the ground, but also can be expanded to include the configuration transformations of the robot when taking multiple steps. Technically, touch sensors can be mounted at the tips of all the spokes. Within the current topology of the robot, if an additional spoke touches the ground

and the topology is about to change, then the new contact point is detected by the touch sensor, its position with respect to the body frame is calculated, and a new ground coordinate system with known configuration is established for the next topology. Repeating Eqs.(1-8), the information about the body's new configuration can be updated based on new joint displacements.

**3.2 Inverse Kinematics.** Inverse kinematics is the reverse development to forward kinematics in which the joint displacements are calculated based on the specified position and orientation of the robot's body. As discussed in Section 3.1, the body's configuration is contained in matrix  $\mathbf{H}_O^B$  with  $\mathbf{x}_b, \mathbf{y}_b$  and  $\mathbf{z}_b$  representing the orientation and  $\mathbf{B}$  the position. The complete form of  $\mathbf{H}_O^B$  is presented as follows:

$$\mathbf{H}_O^B = \begin{bmatrix} x_{bx} & y_{bx} & z_{bx} & B_x \\ x_{by} & y_{by} & z_{by} & B_y \\ x_{bz} & y_{bz} & z_{bz} & B_z \\ 0 & 0 & 0 & 1 \end{bmatrix} \quad (9)$$

which is a 4 by 4 matrix with 16 components.

A rigid free body in 3D space has 6 d.o.f totally. However, the robot's body in "1-1: parallel" cases only has 2 d.o.f because of the kinematic constraints. Therefore, the specification of the body's configuration must be selective and not all 6 d.o.f can be specified arbitrarily. To illustrate this, assume  $\mathbf{H}_O^B$  takes the following numerical form:

$$\mathbf{H}_O^B = \begin{bmatrix} h_{11} & h_{12} & h_{13} & h_{14} \\ h_{21} & h_{22} & h_{23} & h_{24} \\ h_{31} & h_{32} & h_{33} & h_{34} \\ 0 & 0 & 0 & 1 \end{bmatrix} \quad (10)$$

Then, among the 12 components in Eq.(9), only 2 can be chosen as inputs.

The selection of the body's position and orientation is based on the actual requirements for the robot. It is not necessary to investigate all possible combinations of the 2 components out of the 12 candidates. Since the IMPASS is expected to walk and steer on the ground, any two components from its position vector  $\mathbf{B}$  or from the direction vector  $\mathbf{y}_b$  can be utilized as the input variables. The advantage of these combinations is that, the two components from  $\mathbf{B}$  can be used to control the projected position of the robot's body on  $x_o y_o$  plane (ground plane),  $y_o z_o$  plane or  $x_o z_o$  plane. Additionally, the two components from  $\mathbf{y}_b$  can be used to control the heading angle of the robot projected to the ground or the pitch angle projected to  $y_o z_o$  plane.

Assume that  $h_{14}$  and  $h_{24}$  in Eq.(10) are chosen as the input variables, which correspond to  $B_x$  and  $B_y$  in Eq.(9). Then two equations are established as:

$$\begin{cases} B_x = h_{14} \end{cases} \quad (11.1)$$

$$\begin{cases} B_y = h_{24} \end{cases} \quad (11.2)$$

Eqs.(11.1-11.2), Eqs.(5.1-5.3), and Eq.(4) or Eq.(4)\* for “1-1: parallel” or “1-1: skew”, will associatively generate a system of 6 equations with respect to 6 unknowns:  $\theta$ ,  $d_1$ ,  $d_2$ ,  $P_{3x}$ ,  $P_{3y}$  and  $P_{3z}$ . With  $\theta$ ,  $d_1$  and  $d_2$  obtained, the inverse kinematics problem is solved. Note that other combinations of  $h_{ij}$  can also be used to solve for  $\theta$ ,  $d_1$ ,  $d_2$  and the procedures are the same.

However, the computation efficiency of the approach above is not high enough in actual applications. The solutions can be obtained, but with the cost of large amount of time. This is because the number of the unknowns is relatively high (totally 6) and the symbolic form of each component in  $\mathbf{H}_O^B$  is quite complicated, which was obtained after taking the analytical inverse of  $\mathbf{H}_B^O$  in Eq.(8). If the number of the unknowns can be reduced, then the computation efficiency of this approach will be greatly improved.

Revisit the results in Ref. [8]. Both the “1-1: parallel” and the “1-1: skew” contact cases have two continuous and controllable d.o.f.. In such cases, it can be easily observed that as the two spoke wheels rotate about the axle, the body of the IMPASS robot also rotate about the pivot line on the ground. Therefore, the rotational angle of the robot about the pivot line is used in the following analysis to simplify the formulation of inverse kinematics.

“1-1: parallel” cases: Ignoring the body of the robot in such contact cases, the axle and two parallel contacting spokes form a two-branch Spherical-Prismatic parallel mechanism with respect to the ground. As shown in Figure 5(a), the two d.o.f. are the rotation of the axle about the pivoting line  $P_1P_2$  on the ground and the translation of axle along the two contacting spokes. With the two d.o.f. identified, this 2-SP parallel mechanism can be modeled as a virtual serial manipulator. Since the axle and two contacting spokes lie in the same plane, the first joint of the virtual serial manipulator is defined as the rotation of the plane about  $P_1P_2$  and the second joint is defined as the translation of the axle along the spokes within the plane.

The two joint variables are denoted with  $\Theta_1$  and  $D_2$  in Figure 5(a) and the coordinate frames are attached to the virtual joints as demonstrated in Figure 5(b). Again, the fixed coordinate coordinates  $\{x_0, y_0, z_0\}$  on the ground are established following the convention in Sec.3.1, with its origin at  $P_2$ ,  $x_0$  axis pointing to  $P_1$ , and  $z_0$  perpendicular to the ground.

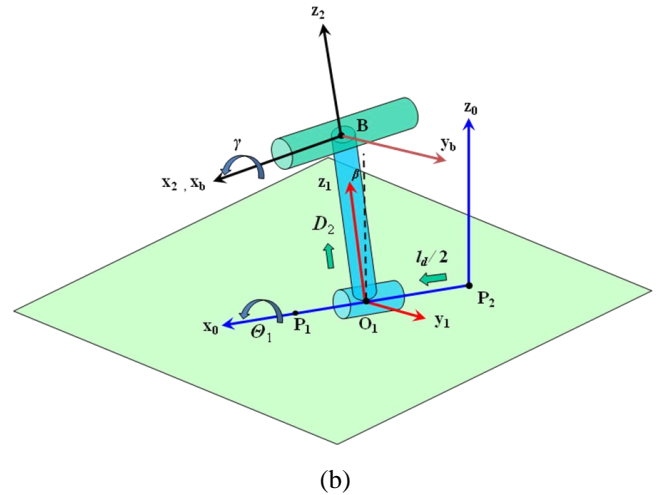
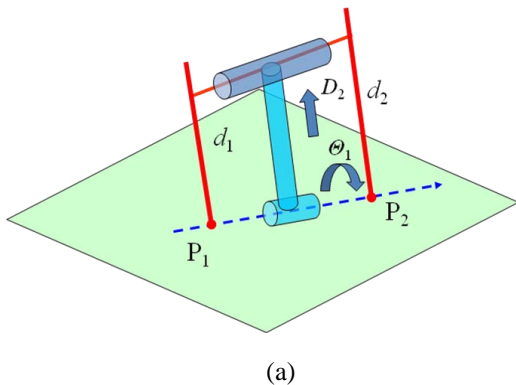


**Figure 5** Virtual serial manipulator model for the “1-1: parallel” contact case

Inspecting Figure 5, the transformation from the ground coordinate  $\{x_0, y_0, z_0\}$  to the body coordinate  $\{x_b, y_b, z_b\}$  is achieved through the following steps. Firstly,  $z_0$  axis is rotated by  $\Theta_1$  about the  $x_0$  axis, i.e. the pivoting line  $P_1P_2$ , such that it is coplanar with the axle and the two contacting spokes. Then, the current origin is translated along the  $x_0$  axis by a linear displacement of  $l_d/2$ , for which  $l_d$  is the distance between the two contact points  $P_1$  and  $P_2$ . The current  $z_0$  axis is rotated by  $\beta$  about the current  $y_0$  axis to be collinear with the  $z_1$  axis. The angle  $\beta$  is determined by the length of the axle and the difference of the two unequal contacting spokes. As for the case of two equal contacting spokes,  $\beta$  is taken as zero. Translating along the  $z_1$  axis for a displacement of  $D_2$ ,  $x_1$  is now collinear with  $x_2$  and  $x_b$ , and the origin is at the central point of the axle. Finally, rotating  $z_2$  axis about the  $x_2$  axis by  $\gamma$ , the body coordinate frame is well established, which exactly matches with the setup in the last section. The complete transformation process can be described by the following equation.

$$\mathbf{H}_O^B = R_x(\Theta_1)T_x(l_d/2)R_y(\beta)T_z(D_2)R_x(\gamma) \quad (12)$$

In this equation,  $\Theta_1$  and  $D_2$  are the two joint variables of the 2 d.o.f. virtual serial manipulator model.  $l_d$  and  $\beta$  are constants predetermined by the lengths of the axle and the contacting spokes, for which:

$$l_d = \sqrt{l_a^2 + \Delta d^2} \quad \text{and} \quad \beta = \arctan(\Delta d / l_a)$$

$\gamma$  is determined by the tangential constraint of the spherical surface at the tail with the ground. Based on Eq.(12), the complete form of  $\mathbf{H}_O^B$  matrix is presented as the Eq.(A) in the Appendix of this paper.

The alternative form of  $\mathbf{H}_O^B$  based on the virtual model of a serial manipulator is very compact and straightforward compared with that derived from taking the inverse of  $\mathbf{H}_B^O$  as shown in Eq.(8). Particularly, when  $\beta$  is taken as zero for the “1-

1: parallel & equal” case, Eq.(12) takes an even simpler form as:

$$\mathbf{H}_o^B = \begin{bmatrix} 1 & 0 & 0 & l_a/2 \\ 0 & \cos(\Theta_1 + \gamma) & -\sin(\Theta_1 + \gamma) & -D_2 \sin \Theta_1 \\ 0 & \sin(\Theta_1 + \gamma) & \cos(\Theta_1 + \gamma) & D_2 \cos \Theta_1 \\ 0 & 0 & 0 & 1 \end{bmatrix} \quad (13)$$

Eq.(A) and Eq.(13) not only can improve the computation efficiency of the inverse kinematics for the “1-1: parallel” cases but also provide more insights into the kinematic configuration when assigning the desired control variables.

“1-1: skew” cases: If the two contacting spokes are skew to each other, another type of two-branch Spherical-Prismatic parallel mechanism is thus generated, as is shown in Figure 6. This parallel mechanism also possesses two d.o.f. based on the mobility analysis in Ref. [6]. The first d.o.f. is similar to the “1-1: parallel” contact case; the body is capable of rotating about the pivoting line  $P_1P_2$  on the ground. The second d.o.f. is caused by changing the lengths of the contacting spokes following the constraint in Eq.(4). It is also a rotational motion about a virtual axis determined by  $e$  and  $l_a$ .

The first d.o.f. is denoted with joint variable  $\Theta_1$ . To make the geometric presentation more straightforward, two auxiliary line segments are created in Figure 6(a). As shown in this figure,  $H_1$  and  $H_2$  are the centers of the left and right spoke wheels respectively. Auxiliary line segment  $H_1P_3$  is parallel and equal to the right contacting spoke and  $H_2P_4$  is parallel and equal to the left contacting spoke. Thus, a rectangle  $P_1P_3P_2P_4$  is generated with the side lengths  $l_a$  and  $c$ , for which  $c^2 = e^2 - l_a^2$ . As the mechanism rotates about the pivoting line on the ground, rectangle  $P_1P_3P_2P_4$  also rotates about  $P_1P_2$  correspondingly. Therefore, joint variable  $\Theta_1$  can be described as the rotational angle between plane  $P_1P_3P_2P_4$  and the ground. The second d.o.f. is denoted with  $\Theta_2$  which occurs within the polyhedron  $P_1H_1P_3P_2H_2P_4$ . For this d.o.f., the axle rotates about a virtual axis as was discussed in Ref. [8]. The direction of this virtual axis is parallel to the axle, as indicated in Figure 6(a).

With the two d.o.f. identified and denoted with the arrows in Figure 6(a), a virtual two-link serial manipulator model for this parallel mechanism can be established. Correspondingly, the coordinate frames are attached to the virtual joints as demonstrated in Figure 6(b). Again, the fixed coordinates  $\{x_0, y_0, z_0\}$  on the ground are established following the convention in Section 3.1, with its origin at  $P_2$ ,  $x_0$  axis pointing to  $P_1$ , and  $z_0$  perpendicular to the ground.

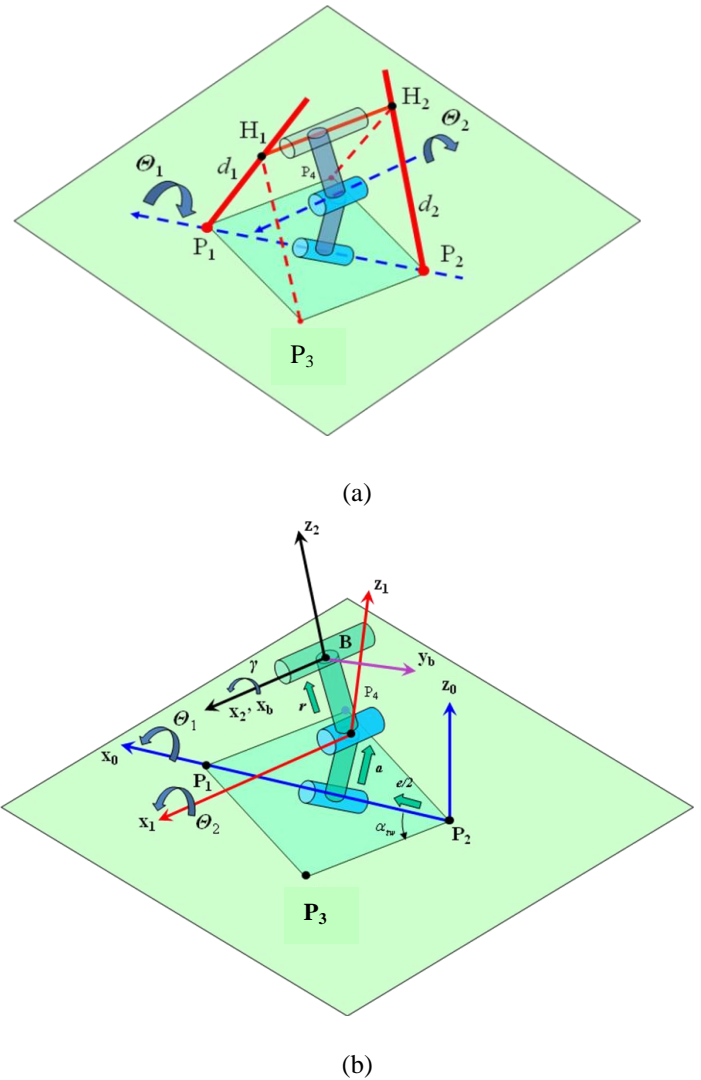


Figure 6 Virtual serial manipulator model for the “1-1: skew” contact case

By inspection, ground coordinate frame  $\{x_0, y_0, z_0\}$  is transformed to the body coordinate frame  $\{x_b, y_b, z_b\}$  through the following steps. First, the origin of  $\{x_0, y_0, z_0\}$  is translated along the  $x_0$  axis by a distance of  $e/2$ . Followed by a rotation of  $\Theta_1$  about  $x_0$ , a rotation of  $\alpha_{tw}$  about the current  $z_0$  and a translation of  $a$  about the same  $z_0$  axis, frame  $\{x_0, y_0, z_0\}$  is then coincident with  $\{x_1, y_1, z_1\}$ . Rotating about the  $x_1$  by  $\Theta_2$  and translating about the current  $z_1$  for a distance  $r$ ,  $\{x_1, y_1, z_1\}$  is transformed to  $\{x_2, y_2, z_2\}$ . The calculation of  $a$  and  $r$  has been discussed in Ref. [8] and  $\alpha_{tw}$  is determined by  $e$  and  $l_a$  as  $\alpha_{tw} = \arcsin[(e^2 - l_a^2)/e]$ . Finally, similar to the “1-1: parallel” cases, rotating about the  $x_2$  axis by  $\gamma$ , the body frame  $\{x_b, y_b, z_b\}$  is achieved. The following matrix equation can be used to describe the complete transformation.

$$\mathbf{H}_O^B = T_x(e/2)R_x(\Theta_1)R_z(\alpha_{tw})T_z(a)R_x(\Theta_1)T_z(r)R_x(\gamma) \quad (14)$$

The closed-form of each component in this matrix is presented in Eq.(B) in the Appendix.

*Determination of  $\gamma$ :* For both the “1-1: parallel” case and “1-1: skew” case,  $\gamma$  can be determined using the tangential constraints of the spherical surface at the tail and the ground plane. Assume the center of the sphere is located at  $[C_a, C_b, C_c]$  in the body coordinate system  $\{x_b, y_b, z_b\}$  and the radius is  $R$ , then the equation of the spherical surface can be written as:

$$(x_b - C_a)^2 + (y_b - C_b)^2 + (z_b - C_c)^2 = R^2$$

Represent the global coordinates of the spherical center with  $[C_{a,G}, C_{b,G}, C_{c,G}]$ , then  $[C_{a,G}, C_{b,G}, C_{c,G}]$  can be obtained from:

$$\begin{bmatrix} C_{a,G} \\ C_{b,G} \\ C_{c,G} \\ 1 \end{bmatrix} = \mathbf{H}_O^B \begin{bmatrix} C_a \\ C_b \\ C_c \\ 1 \end{bmatrix}$$

The equation of the spherical surface can be rewritten in ground coordinate frame  $\{x_0, y_0, z_0\}$  as:

$$(x - C_{a,G})^2 + (y - C_{b,G})^2 + (z - C_{c,G})^2 = R^2 \quad (15)$$

Assume the tangential point of the spherical surface and the ground plane is  $[x_t, y_t, z_t]$ , then the equation of the tangential plane is:

$$(x_t - C_{a,G})(x - x_t) + (y_t - C_{b,G})(y - y_t) + (z_t - C_{c,G})(z - z_t) = 0$$

Consider the fact that the tangential point  $[x_t, y_t, z_t]$  also lies on the ground plane of  $z = 0$ ,  $z_t = 0$  can be inferred and the equation above is further simplified as:

$$(x_t - C_{a,G})(x - x_t) + (y_t - C_{b,G})(y - y_t) - C_{c,G}z = 0 \quad (16)$$

Compare Eq.(16) with the equation of the ground plane  $z = 0$ , two equations can be simply derived as:

$$\begin{cases} x_t - C_{a,G} = 0 \\ y_t - C_{b,G} = 0 \end{cases} \quad (17)$$

Moreover,  $[x_t, y_t, z_t]$  with  $z_t = 0$  has to satisfy Eq.(15), such that

$$(x_t - C_{a,G})^2 + (y_t - C_{b,G})^2 + C_{c,G}^2 = R^2 \quad (18)$$

Considering Eq.(17) and (18) associatively, the equation to solve for  $\gamma$  is obtained straightforwardly as:

$$C_{c,G} = \pm R \quad (19)$$

with  $+R$  for the sphere contacts the ground plane above and  $-R$  for the sphere below which could be discard.

As a summary, the closed-form matrix expressions of Eq.(12) and (14) are based on the two virtual serial manipulator models. Compared with Eq.(8), both the complexity of the symbolic form of each component and the number of unknown variables are greatly reduced, thus improving the computation

efficiency and providing more insights when solving the inverse kinematics problems.

#### 4. NUMERICAL EXAMPLES

Examples based on numerical simulations are presented in this section as a validation to the development in Section 3. The equations are solved using the embedded algorithm in *Mathematica* and the solutions are plotted.

The basic geometric parameters of the IMPASS model are listed in the following table.

**Table 1** Basic geometric parameters of IMPASS

Length of the axle $l_a$	16 (in)
Center of the spherical surface with respect to $\{x_b, y_b, z_b\}$	[0, -35, 14] (in)
Radius of the spherical surface	21 (in)
Total length of a spoke	23.5 (in)

“1-1: parallel” case: The initial joint displacements are chosen as:  $\theta = 0.5$  (rad), right spoke length  $d_1 = 14$  (in) and left spoke length  $d_2 = 10$  (in). Applying Eqs.(1-5), within decent amount of time, the solutions to the tangential and contact point  $P_3$  are obtained as :

$$[-4.709, -37.004, -6.367] \text{ and } [3.637, -15.124, 19.720]$$

The second solution can be eliminated because it corresponds to a tangential point at the upper portion of the spherical surface. Using Eqs.(6-8), the matrix  $\mathbf{H}_O^B$  is determined now as:

$$\mathbf{H}_O^B = \begin{bmatrix} 0.970 & -0.116 & -0.213 & 5.336 \\ 0.093 & 0.989 & -0.119 & 4.438 \\ 0.224 & 0.095 & 0.970 & 10.762 \\ 0 & 0 & 0 & 1 \end{bmatrix} \quad (20)$$

Using the values contained in Eq.(20), the configuration of the IMPASS model is plotted in Figure 7. Note that in this figure, the partial spherical surface at IMPASS’ tail is represented with a complete transparent sphere. This is just to illustrate the reason why the additional solution can be eliminated.

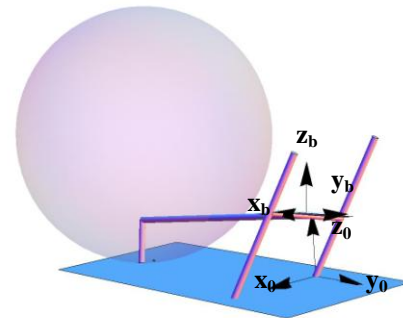


**Figure 7** Forward kinematics solution (1-1: parallel & unequal)

Since  $\mathbf{H}_O^B$  in Eq.(12) becomes a matrix containing values calculated based on the forward kinematics in Section 3.1, its components can now be utilized to validate the formulation of inverse kinematics in Section 3.2.

Assume  $B_x$  and  $B_y$  in Eq.(9) are chosen as the inputs, then two equations based on Eq.(A) can be established as:

$$\begin{cases} l_d / 2 + D_2 \sin \beta = 5.336 & (21.1) \\ -D_2 \cos \beta \sin \Theta_1 = 4.438 & (21.2) \end{cases}$$

Then,  $D_2$  is solved firstly as  $D_2 = 12$ ; and from Eq.(21.2),  $\Theta_1$  is determined as  $\Theta_1 = -0.391$ . The term of  $\sin \Theta_1$  may allow for multiple solutions. However, since the geometric interpretation of  $\Theta_1$  is the angle between the plane of the ground and the plane containing the axle and contacting spokes, an angle greater than  $\pi/2$  or smaller than  $-\pi/2$  is unlikely to happen in reality. A reasonable range for  $\Theta_1$  could be  $[-\pi/2, \pi/2]$ , and the solutions out of this range can be discarded.

With  $\Theta_1 = -0.391$  and  $D_2 = 12$ , Eq.(19) can now be used to solve for  $\gamma$  and the two solutions are listed as:

$$\gamma_1 = -2.077 \quad (22.1)$$

$$\gamma_2 = 0.5 \quad (22.2)$$

The first solution corresponds to the case in which the upper portion of the spherical surface contacts the ground, while the second solution corresponds to the lower portion. Similar to  $\Theta_1$ , a reason range for  $\gamma$  could be  $[-\pi/2, \pi/2]$ , then the unfeasible solution  $\gamma_1 = -2.077$  can be discarded and only one feasible solution is achieved. With  $\Theta_1$ ,  $D_2$  and  $\gamma$  obtained, the actual joint displacements are then determined from the following equations:

$$\begin{aligned} \theta &= \gamma \\ d_1 &= D_2 + \Delta d / 2 \\ d_2 &= D_2 - \Delta d / 2 \end{aligned} \quad (23)$$

And the results are  $\Theta_1 = 0.5$ ,  $d_1 = 14$  and  $d_2 = 10$ , which exactly match with the initial setup.

“1-1: skew” Case: The basic geometric parameters of the IMPASS model still follow Table 1 and the initial setup of the actual joint displacements is:  $\theta = 0.1$  (rad),  $d_1 = 10$  (in) and  $d_2 = 10$  (in). The forward kinematics is solved following the procedures in Section 3.1 and the current configuration for this case is plotted in Figure 8.

Correspondingly, the configuration matrix  $\mathbf{H}_O^B$  for the robot’s body in Figure 8 is:

$$\mathbf{H}_O^B = \begin{bmatrix} 0.848 & -0.483 & -0.218 & 9.434 \\ 0.467 & 0.876 & -0.126 & -4.109 \\ 0.251 & 0.005 & 0.968 & 7.623 \\ 0 & 0 & 0 & 1 \end{bmatrix} \quad (24)$$

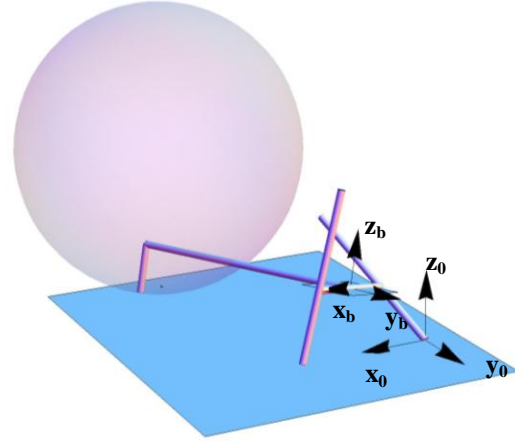


Figure 8 Forward kinematics solution (1-1:skew)

Assume  $y_{by}$  and  $y_{bz}$  in Eq.(9) are chosen as the inputs, then the equations system based on Eq.(B) and (19) can be established as:

$$\begin{cases} \cos \alpha_w \cos \Theta_1 \cos (\Theta_2 + \gamma) - \sin \Theta_1 \sin (\Theta_2 + \gamma) = 0.876 & (25.1) \\ \cos \alpha_w \sin \Theta_1 \cos (\Theta_2 + \gamma) + \cos \Theta_1 \sin (\Theta_2 + \gamma) = 0.005 & (25.2) \end{cases}$$

$$C_{c,c}(\Theta_1, \Theta_2, \gamma) = \cos \Theta_1 [a + r \cos \Theta_2 + C_c \cos (\Theta_2 + \gamma) + C_c \sin (\Theta_2 + \gamma)] \quad (25.2)$$

$$+ \sin \Theta_1 [C_a \sin \alpha_w + \cos \alpha_w (C_b \cos (\Theta_2 + \gamma) - r \sin \Theta_2 - C_c \sin (\Theta_2 + \gamma))] = R \quad (25.3)$$

Replace  $\Theta_2 + \gamma$  with  $\Theta_3$  such that the Eq.(25.2) and (25.3) can associatively solve for two unknowns  $\Theta_1$  and  $\Theta_3$  firstly. And the solutions are as follows:

$$\begin{cases} \Theta_{1,1} = 2.659 \\ \Theta_{3,1} = -2.718 \end{cases} \quad (26.1)$$

$$\begin{cases} \Theta_{1,2} = -2.647 \\ \Theta_{3,2} = 2.717 \end{cases} \quad (26.2)$$

$$\begin{cases} \Theta_{1,3} = 0.494 \\ \Theta_{3,3} = -0.424 \end{cases} \quad (26.3)$$

$$\begin{cases} \Theta_{1,4} = -0.483 \\ \Theta_{3,4} = 0.423 \end{cases} \quad (26.4)$$

The solutions in Eq.(26.1) and (26.2) can be eliminated because they are out of the range of  $[-\pi/2, \pi/2]$ . Using Eq.(25.3) and the results in Eq.(26.3) and (26.4),  $\Theta_2$  is determined as:

$$\begin{aligned} \Theta_{2,1} &= -0.857 \\ \Theta_{2,2} &= 0 \\ \Theta_{2,3} &= 0.865 \\ \Theta_{2,4} &= -0.028 \end{aligned} \quad (27)$$

With  $\Theta_1$ ,  $\Theta_2$  and  $\gamma$  solved, the 12 components in matrix  $\mathbf{H}_O^B$  can be completely determined. Thus, the actual joint variables of the “1-1: skew” case  $d_1$ ,  $d_2$  and  $\theta$ , can be calculated as:

$$\begin{aligned}
d_1 &= \|\mathbf{P}_1 - \mathbf{H}_1\| \\
d_2 &= \|\mathbf{P}_2 - \mathbf{H}_2\| \\
\theta &= \text{VectorAngle}(\mathbf{y}_b, \mathbf{P}_1 \mathbf{H}_1) - \pi / 2
\end{aligned}
\tag{28}$$

Therefore, the results based on values in Eq.(26.3,26.4) and (27) are:

$$\begin{cases}
d_{1,1} = 11.495 \\
d_{2,1} = 6.695 \\
\theta_1 = 0.529
\end{cases}
\tag{29.1}$$

$$\begin{cases}
d_{1,2} = 10 \\
d_{2,2} = 10 \\
\theta_2 = 0.1
\end{cases}
\tag{29.2}$$

$$\begin{cases}
d_{1,3} = 6.661 \\
d_{2,3} = 11.499 \\
\theta_3 = 0.515
\end{cases}
\tag{29.3}$$

$$\begin{cases}
d_{1,4} = 10.079 \\
d_{2,4} = 9.919 \\
\theta_4 = 0.961
\end{cases}
\tag{29.4}$$

By inspection, all four solutions are feasible and the second solution in Eq.(29.2) matches with the initial setup.

## 6. CONCLUSIONS AND FUTURE RESEARCH

This paper presents the concept of parallel locomotion mechanisms, and utilizes the IMPASS robot as an example to discuss the forward and inverse kinematics analysis for such mechanisms. The cases of the IMPASS robot with two spokes and the tail contacting the ground are sufficiently addressed, while other contacts cases can be handled through the similar procedures. The formulation of the closed-form solutions is validated with numerical simulations. For this particular locomotion mechanism, the forward kinematics can reach the unique solution. However, the inverse kinematics usually results in multiple solutions. An elimination criterion based on the effective region of the spherical surface and the range of the joint displacements can be used to discard those unfeasible solutions. But to reach the unique solution, additional information about the configuration of the robot's body must be given.

The forward kinematics lays the theoretical foundation for the remote monitoring of the robot's motion on smooth terrains. And the inverse kinematics can be used in the control of the robot's body in a specific contact case. The closed-form kinematics solutions allow themselves to be used efficiently in real-time operations. Besides these topics, future research should also include the motion planning algorithm of tracking a given path on the ground, and the design optimization of the surface geometry at the tail to adapt to various terrains.

## ACKNOWLEDGMENTS

The support of the National Science Foundation under Grant No. 0535012 is gratefully acknowledged. The authors would also like to thank Shawn Kimmel, J. Blake Jeans and the senior design teams from 2008 to 2009 for their contribution in the development of IMPASS prototypes.

## REFERENCES

- [1] Raibert, M. H., 1986, *Legged Robots That Balance*, The MIT Press.
- [2] Ren, P., 2010, "Kinematics Analysis of Two Parallel Locomotion Mechanisms," Ph.D Virginia Tech, Blacksburg, VA.
- [3] Ren, P., and Hong, D., 2009, "Triple Stance Phase Displacement Analysis with Redundant and Nonredundant Sensing in a Novel Three-Legged Mobile Robot Using Parallel Kinematics," *Journal of Mechanisms and Robotics*, 1(Copyright 2009, The Institution of Engineering and Technology), pp. 041001 (11 pp.).
- [4] Laney, D., and Hong, D., 2005, "Kinematic Analysis of a Novel Rimless Wheel with Independently Actuated," *Proc. 29th ASME Mechanisms and Robotics Conference*, Long Beach, CA, United states, 7 B, pp. 609-614.
- [5] Laney, D., and Hong, D., 2006, "Three-Dimensional Kinematic Analysis of the Actuated Spoke Wheel Robot," *Proc. 30th ASME Mechanisms and Robotics Conference*, Philadelphia, PA, United states, 2006.
- [6] Wang, Y., Ren, P., and Hong, D., 2008, "Mobility and Geometrical Analysis of a Two Actuated Spoke Wheel Robot Modeled as a Mechanism with Variable Topology," *Proc. 32nd ASME Mechanisms and Robotics Conference*, Brooklyn, New York.
- [7] Ren, P., Jeans, J. B., and Hong, D., 2009, "Kinematic Analysis and Experimental Verification on the Steering Characteristics of a Two Actuated Spoke Wheel Robot with a Tail," *Proc. 33rd ASME Mechanisms and Robotics Conference*, San Diego, California, USA.
- [8] Ren, P., Wang, Y., and Hong, D., 2008, "Three-Dimensional Kinematic Analysis of a Two Actuated Spoke Wheel Robot Based on Its Equivalency to a Serial Manipulator," *Proc. 32nd ASME Mechanisms and Robotics Conference*, Brooklyn, New York.
- [9] Saranli, U., Buehler, M., and Koditschek, D. E., 2001, "Rhex: A Simple and Highly Mobile Hexapod Robot," *International Journal of Robotics Research*, 20(7), pp. 616-31.
- [10] Quinn, R. D., Nelson, G. M., Bachmann, R. J., Kingsley, D. A., Offi, J. T., Allen, T. J., and Ritzmann, R. E., 2003, "Parallel Complementary Strategies for Implementing Biological Principles into Mobile Robots," 22, pp. 169-186.
- [11] Velimirovic, A., Velimirovic, M., Hugel, V., Iles, A., and Blazevic, P., 1998, "A New Architecture of Robot with Wheels-with-Legs (Wwl)," *Proc. AMC'98 - Coimbra. 1998 5th International Workshop on Advanced Motion Control*.

**APPENDIX**

Closed-form configuration matrix  $\mathbf{H}_O^B$  for inverse kinematics analysis:

“1-1: parallel”

$$\mathbf{H}_O^B = \begin{bmatrix} \cos \beta & \sin \beta \sin \gamma & \cos \gamma \sin \beta & l_d / 2 + D_2 \sin \beta \\ \sin \Theta_1 \sin \beta & \cos \Theta_1 \cos \gamma - \cos \beta \sin \Theta_1 \sin \gamma & -\cos \beta \cos \gamma \sin \Theta_1 - \cos \Theta_1 \sin \gamma & -D_2 \cos \beta \sin \Theta_1 \\ -\cos \Theta_1 \sin \beta & \sin \Theta_1 \cos \gamma + \cos \beta \cos \Theta_1 \sin \gamma & \cos \Theta_1 \cos \beta \cos \gamma - \sin \Theta_1 \sin \gamma & D_2 \cos \Theta_1 \cos \beta \\ 0 & 0 & 0 & 1 \end{bmatrix} \quad (A)$$

“1-1: skew”

$$\mathbf{H}_O^B = \begin{bmatrix} \cos \alpha_{tw} & -\cos(\Theta_2 + \gamma) \sin \alpha_{tw} & & \\ \cos \Theta_1 \sin \alpha_{tw} & \cos \alpha_{tw} \cos \Theta_1 \cos(\Theta_2 + \gamma) - \sin \Theta_1 \sin(\Theta_2 + \gamma) & & \\ \sin \Theta_1 \sin \alpha_{tw} & \cos \alpha_{tw} \sin \Theta_1 \cos(\Theta_2 + \gamma) + \cos \Theta_1 \sin(\Theta_2 + \gamma) & & \\ 0 & 0 & & \\ & \sin(\Theta_2 + \gamma) \sin \alpha_{tw} & e / 2 + r \sin \alpha_{tw} \sin \Theta_2 & \\ -\cos \alpha_{tw} \cos \Theta_1 \sin(\Theta_2 + \gamma) - \sin \Theta_1 \cos(\Theta_2 + \gamma) & -(a + r \cos \Theta_2) \sin \Theta_1 - r \cos \alpha_{tw} \cos \Theta_1 \sin \Theta_2 & & \\ \dots & -\cos \alpha_{tw} \sin \Theta_1 \sin(\Theta_2 + \gamma) + \cos \Theta_1 \cos(\Theta_2 + \gamma) & (a + r \cos \Theta_2) \cos \Theta_1 - r \cos \alpha_{tw} \sin \Theta_1 \sin \Theta_2 & \\ & 0 & 1 & \end{bmatrix} \quad (B)$$